APL Materials

RESEARCH ARTICLE | DECEMBER 13 2024

Noncollinear polar magnet $Fe_2(SeO_3)_3(H_2O)_3$ with inequivalent Fe^{3+} sites

Special Collection: Emerging Leaders in Materials Science

Ebube E. Oyeka ; Xudong Huai ; Madalynn Marshall ; Michał J. Winiarski ; Artur Błachowski ; Huibo Cao ; Thao T. Tran

Check for updates

APL Mater. 12, 121115 (2024)
https://doi.org/10.1063/5.0241243

View Online
Export Citation

Articles You May Be Interested In

Quasi-doublets of non-Kramers Ho^{3+} ion and magnetic ordering of holmium francisite-analog $Cu_3Ho(SeO_3)_2O_2Cl$

Low Temp. Phys. (December 2021)

Effect of Co doping on structural and magnetic properties of kagome like La based cuprate francisite $Cu_3La(SeO_3)_2O_2Cl$

J. Appl. Phys. (May 2023)

Electron spin resonance insight into broadband absorption of the $Cu_3Bi(SeO_3)_2O_2Br$ metamagnet

AIP Advances (March 2016)

16 December 2024 14:27:01

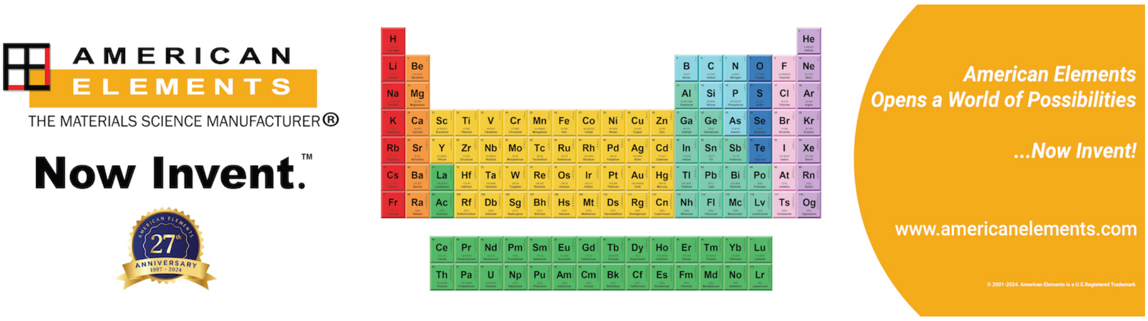

AMERICAN ELEMENTS
THE MATERIALS SCIENCE MANUFACTURER®
Now Invent.™
27th ANNIVERSARY 1997 - 2024
American Elements Opens a World of Possibilities
...Now Invent!
www.americanelements.com
© 2001-2024. American Elements is a U.S. Registered Trademark

AIP Publishing

Noncollinear polar magnet $Fe_2(SeO_3)_3(H_2O)_3$ with inequivalent Fe^{3+} sites

Cite as: APL Mater. 12, 121115 (2024); doi: 10.1063/5.0241243
Submitted: 29 September 2024 • Accepted: 23 November 2024 •
Published Online: 13 December 2024

View Online Export Citation CrossMark

Ebube E. Oyeka,[1] **Xudong Huai,**[1] **Madalynn Marshall,**[2] **Michał J. Winiarski,**[3] **Artur Błachowski,**[4] **Huibo Cao,**[2] **and Thao T. Tran**[1,a)]

AFFILIATIONS

[1] Department of Chemistry, Clemson University, Clemson, South Carolina 29634, USA
[2] Neutron Scattering Division, Oak Ridge National Laboratory, Oak Ridge, Tennessee 37831, USA
[3] Faculty of Applied Physics and Mathematics and Advanced Materials Center, Gdansk University of Technology, ul. Narutowicza 11/12, 80-233 Gdansk, Poland
[4] Faculty of Geology, Geophysics and Environmental Protection, AGH University of Krakow, al. Mickiewicza 30, 30-059 Kraków, Poland

Note: This paper is part of the Special Topic titled Emerging Leaders in Materials Science.

[a)] **Author to whom correspondence should be addressed:** thao@clemson.edu

ABSTRACT

The emergence of novel magnetic states becomes more likely when the inversion symmetry of the crystal field, relative to the center between two spins, is broken. We propose that placing magnetic spins in inequivalent sites in a polar lattice can promote a realization of nontrivial magnetic states and associated magnetic properties. To test our hypothesis, we study $Fe_2(SeO_3)(H_2O)_3$ as a model system that displays two distinct Fe(1) and Fe(2) magnetic sites in a polar structure ($R3c$ space group). At low fields $\mu_0 H \le 0.06$ T, the material undergoes an antiferromagnetic ordering with $T_{N1} = 77$ K and a second transition at $T_{N2} \approx 4$ K. At $\mu_0 H \ge 0.06$ T and 74 K $\le T \le$ 76 K, a positive entropy change of ~0.12 mJ mol^{-1} K^{-1} can be associated with a metamagnetic transition to possibly nontrivial spin states. At zero field, Fe(1) is nearly fully ordered at $T \approx 25$ K, while Fe(2) features magnetic frustration down to $T = 4$ K. The magnetic ground state, a result corroborated by single-crystal neutron diffraction and ^{57}Fe Mössbauer spectroscopy, is a noncollinear antiparallel arrangement of ferrimagnetic Fe(1)–Fe(2) dimers along the c-axis. The results demonstrate that placing distinct magnetic sites in a polar crystal lattice can enable a new pathway to modifying spin, orbital, and lattice degrees of freedom for unconventional magnetism.

© 2024 Author(s). All article content, except where otherwise noted, is licensed under a Creative Commons Attribution-NonCommercial-NoDerivs 4.0 International (CC BY-NC-ND) license (https://creativecommons.org/licenses/by-nc-nd/4.0/). https://doi.org/10.1063/5.0241243

16 December 2024 14:27:01

INTRODUCTION

The prediction and discovery of complex, new magnetic states are essential to advancing next-generation information technology.[1–9] Breaking inversion symmetry can stabilize nontrivial magnetic states, some of which are characterized by metamagnetic transitions.[10–21] In the metamagnetic phase boundary, a paramagnetic or antiferromagnetic (AFM) ground state transforms into a spin-polarized state when the applied field overcomes the exchange interaction between the collinear spin arrangements.[16,22] This is accompanied by a field-induced first-order phase transition between the two states.[23,24]

Metamagnetic behaviors have been demonstrated in polar antiferromagnets with complex magnetic ground states, such as $Ca_3Ru_2O_7$, $Fe(IO_3)_3$, $BaCoSiO_4$, and $Fe_2Mo_3O_8$, and in Cu_2OSeO_3, $VOSe_2O_5$, and GaV_4S_8 skyrmion hosts.[16,21,23,25–34] These materials often have unique spin orientations along different axial directions or feature inequivalent magnetic cations at different crystallographic sites.

$Ca_3Ru_2O_7$ ($Bb2_1m$ space group) possesses AFM in the ground state. The spin moments align in a ferromagnetic (FM) fashion within the RuO_6 bilayer and couple antiferromagnetically between bilayers.[16,35] Under the applied magnetic field along the polar b-axis, the AFM order is destabilized, and a spin-spiral modulated

© Author(s) 2024

AFM–FM state emerges.[16] In $Fe(IO_3)_3$ ($P6_3$), the ground-state magnetic structure is described as AFM ordering in the *ab*-plane and an incommensurate FM spiral along the *c*-direction with sizable asymmetric exchange interaction.[26]

$Fe_2Mo_3O_8$ ($P6_3mc$) features two types of Fe^{2+} cations in tetrahedral and octahedral ligand fields with unequal spin moments.[27,28,36] In this material, collinear spins align antiparallel between the different crystallographic sites, giving rise to AFM ordering in the ground state and a ferrimagnetic spin arrangement under applied fields.[28,37]

Skyrmion hosts, such as Cu_2OSeO_3, $VOSe_2O_5$, and GaV_4S_8, also display site-inequivalent magnetic cations. In Cu_2OSeO_3 ($P2_13$), the Cu^{2+} cations occupying different crystallographic sites form CuO_5 square pyramids and trigonal bipyramid units in a 3:1 ratio.[29] As a result, its magnetic ground state is a helix with ferrimagnetic three-up and one-down-spin clusters.[30,38] $VOSe_2O_5$ crystallizes in the $P4cc$ space group with three unique V^{4+} cations that form linear chains of VO_6 octahedra along the *c*-axis.[31] AC susceptibility measurement reveals three transition temperatures in this material.[31] Powder neutron diffraction experiment and density functional theory computation suggest three-up and one-down ferrimagnetic-type spin ordering.[31,32] GaV_4S_8 ($R3m$ space group) features V_4 clusters composed of two inequivalent V^{4+} cations in a 3:1 ratio.[33] The spin moment of each distinctive V^{4+} site aligns differently. One aligns parallel to the hexagonal *c*-axis, while the other is canted outwards from the center of the cluster, giving rise to a ferromagnetically ordered ground state.[33,39,40]

In the search for additional understanding and tunability of polar magnets, we investigate $Fe_2(SeO_3)(H_2O)_3$ ($R3c$ space group), which displays two site-inequivalent Fe^{3+} cations in *fac*-$Fe(1)O_3(H_2O)_3$ and $Fe(2)O_6$ octahedra. $Fe_2(SeO_3)(H_2O)_3$ exhibits complex magnetic properties. Previous electron spin resonance spectroscopy and magnetization studies at $\mu_0 H = 0.1$ T suggested a paramagnetic spin configuration down to $T = 2$ K with a Curie–Weiss anomaly at $T \approx 40$ K, which was attributed to a possible change in the spin state from Fe^{3+} ($S = 5/2$) to Fe^{2+} ($S = 2$).[41] Here, we study the contributions of spin, orbital, and lattice symmetry of $Fe_2(SeO_3)(H_2O)_3$ to its magnetic and thermodynamic properties. We supplement these experiments with ^{57}Fe Mössbauer spectroscopy, single-crystal neutron diffraction, and density functional theory (DFT) calculations to improve our understanding of this system.

RESULTS AND DISCUSSION

$Fe_2(SeO_3)_3(H_2O)_3$ crystallizes in a noncentrosymmetric polar $R3c$ space group [Figs. 1(a) and 1(b)]. The Fe^{3+} ($S = 5/2$) magnetic cations occupy two inequivalent crystallographic sites [Fe(1) and Fe(2)] with different ligand fields, *fac*-$Fe(1)O_3(H_2O)_3$ and $Fe(2)O_6$. These two Fe^{3+} magnetic units are connected through $(SeO_3)^{2-}$ groups and Fe(1)–O–H–Fe(2) hydrogen bonds. The overlap between the Fe-*d* states and the $(SeO_3)^{2-}$ and H_2O linkers having stereoactive lone-pair electrons can improve the bandwidth around the Fermi level. The hydrogen bond between the two Fe(1) and Fe(2) magnetic ions can enhance their spin interactions.

To investigate the magnetic behavior of the material, we performed temperature-dependent magnetization experiments. $Fe_2(SeO_3)_3(H_2O)_3$ exhibits complex magnetic properties. At low magnetic field $\mu_0 H = 0.01$ T, the material undergoes an antiferromagnetic ordering at $T_{N1} = 77$ K and a second transition at $T_{N2} \approx 4$ K [Fig. 1(c)].

To determine the effective moment of the magnetic cation and the nature of the exchange coupling, magnetic susceptibility data $T > T_{N1}$ 77 K were analyzed using the Curie–Weiss law [Fig. 1(c)],

$$\chi(T) = \frac{C}{T - \theta_{CW}} + \chi_0, \tag{1}$$

16 December 2024 14:27:01

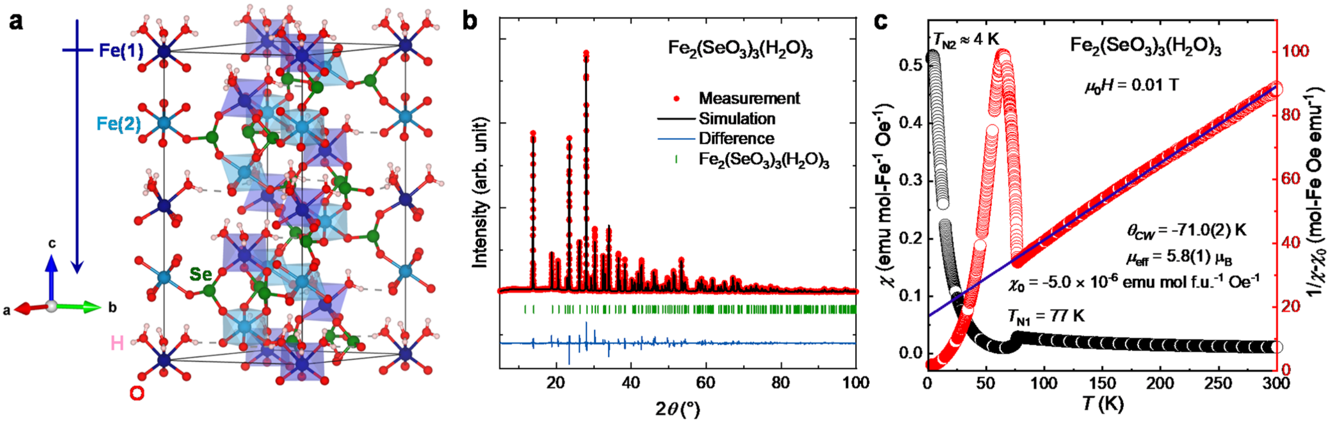

FIG. 1. (a) Crystal structure of $Fe_2(SeO_3)_3(H_2O)_3$ consisting of corner-shared *fac*-$Fe(1)O_3(H_2O)_3$ and $Fe(2)O_6$ distorted octahedra and $(SeO_3)^{2-}$ trigonal pyramid. The polar *fac*-$Fe(1)O_3(H_2O)_3$ octahedra are aligned along the *c*-axis to give macroscopic electric polarization. (b) Rietveld refinement of powder XRD data. The powder XRD is consistent with the single-crystal data, and no impurity phase was observed. (c) (Black) Magnetic susceptibility and (red) Curie–Weiss fit of $1/\chi - \chi_0$ against temperature in the paramagnetic region at $\mu_0 H = 0.01$ T.

© Author(s) 2024

where C is the Curie constant, θ_{CW} is the Curie–Weiss temperature, and χ_0 is the temperature-independent contribution to the susceptibility, which includes the small diamagnetic signals of the electron core and the sample holder.[42] A linear correlation of $1/(\chi - \chi_0)$ vs T indicates the Curie–Weiss behavior. The effective magnetic moment μ_{eff} per Fe^{3+} was estimated using the relation,

$$\mu_{eff} = \sqrt{\left(\frac{3k_B}{N_A \mu_B^2}\right) C}, \tag{2}$$

where N_A is the Avogadro number and k_B is the Boltzmann constant.

The Curie–Weiss temperature was estimated from the intercept of the linear fit to be $\theta_{CW} = -71.0(2)$ K, indicating sizable antiferromagnetic exchange interactions between the magnetic spins. The effective magnetic moment of Fe^{3+} $\mu_{eff} = 5.8(1)\ \mu_B$, close to the ideal $g[S(S+1)]^{1/2} = 5.92\ \mu_B$ value expected for high-spin $S = 5/2$.

To study the field-induced magnetic transitions, DC magnetization measurements under a series of applied fields 0.0025 T $\leq \mu_0 H \leq 0.2$ T were performed to probe entropy change near the ordering temperature 73 K $\leq T_{N1} \leq$ 79 K. Field-driven first-order phase transitions show up as peaks or valleys in the magnetoentropic curve.[43–45] Figure 2(a) shows how the magnetization evolves as a function of temperature. As the magnetic field increases, T_{N1} shifts slightly to a lower temperature, and the AFM ordering suppresses. The isothermal entropy change upon magnetization ΔS_M (H, T) is obtained from the Maxwell relation [Eq. (3)],

$$(dM/dT)_H = (dS/dH)_T, \tag{3}$$

where S is the total entropy, H is the magnetic field, M is the magnetization, and T is the temperature. ΔS_M (H, T) is derived using the following equation:

$$\Delta S_M(H,T) = \int_0^H \left(\frac{dM}{dT}\right)_{H'} dH'. \tag{4}$$

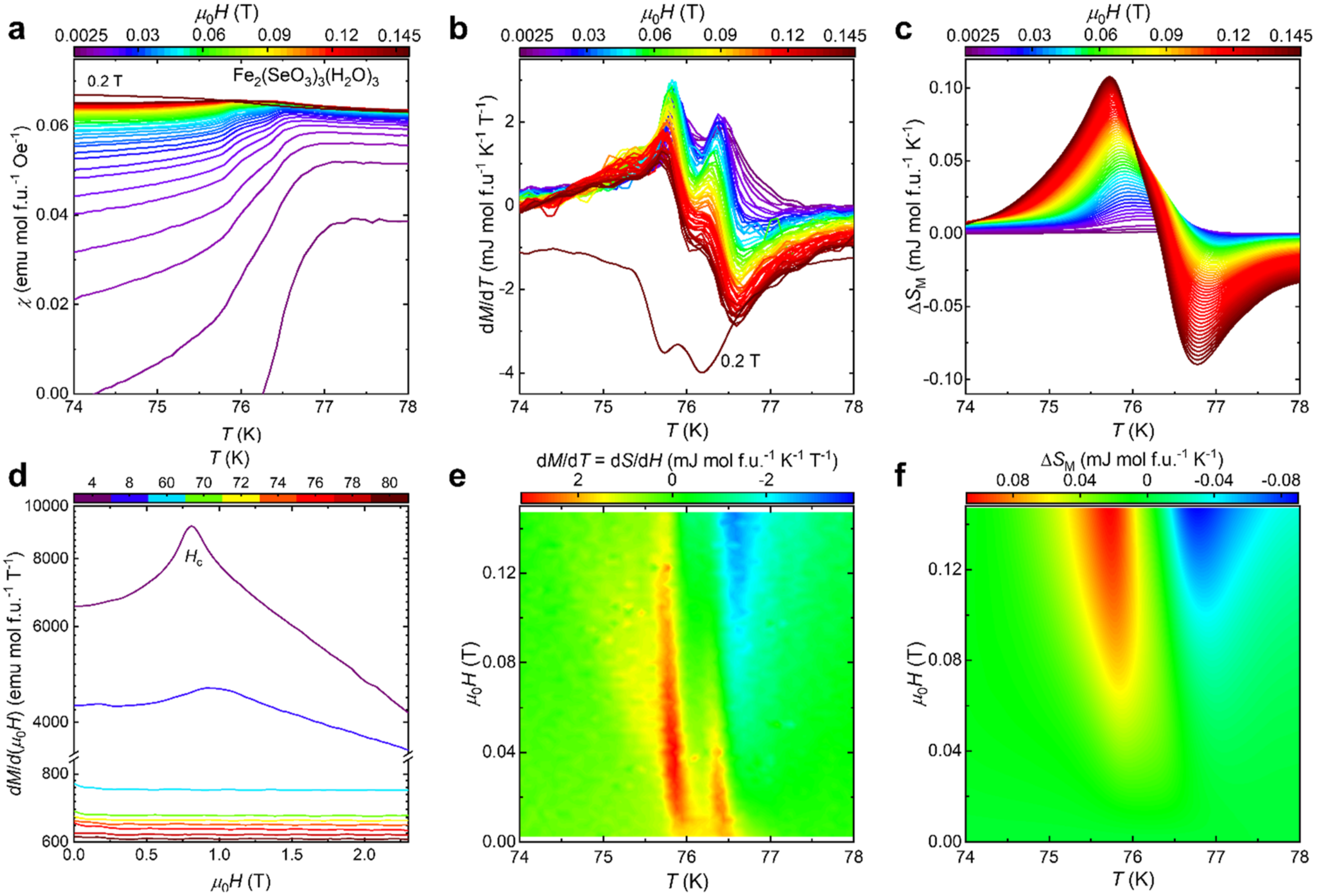

FIG. 2. $Fe_2(SeO_3)_3(H_2O)_3$ (a) $\chi(T)$ $[M(T)/(\mu_0 H)]$ curves at different magnetic fields. (b) First derivative of magnetization with respect to the temperature, $dM/dT = dS/dH$. (c) Isothermal magnetic entropy change ΔS_M under a series of applied fields 0 T $\leq \mu_0 H \leq$ 0.145 T. (d) First derivative of magnetization with respect to field dM/dH curve. (e) and (f) magnetoentropic map near the ordering temperature T_{N1} = 77 K. (e) A map of $dM/dT = dS/dH$ showing ridges and valleys indicating first-order transitions. (f) ΔS_M map.

16 December 2024 14:27:01

© Author(s) 2024

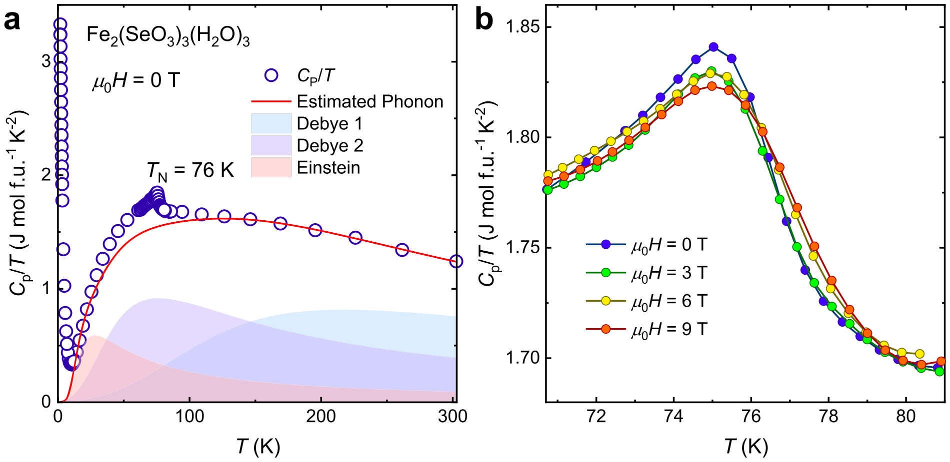

FIG. 3. (a) Molar heat capacity over temperature (C_p/T) vs temperature for $Fe_2(SeO_3)_3(H_2O)_3$. The anomalies at $T = 76$ K and onset temperature $T = 11$ K are consistent with the ordering temperatures of the material. The phase transitions are incomplete down to $T = 2$ K. The calculated phonon was best fitted using a combination of two Debye and one Einstein mode. The sum of the oscillators 19(3) is lower than the expected value of 23, likely due to the presence of the high-frequency optical modes from covalent SeO_3 and H_2O ligands. (b) Molar heat capacity measured at different magnetic fields. The magnetic transition temperature changes slightly with the applied magnetic field up to 9 T.

The dM/dT and ΔS_M plots of $Fe_2(SeO_3)_3(H_2O)_3$ are depicted in Figs. 2(b) and 2(c). The two peaks in the dM/dT curves at 75 K $\le T \le$ 77.5 K indicate field-induced first-order magnetic transitions. In the dM/dT map [Fig. 2(e)], the red ridges at $T \approx 76$ K are associated with magnetic phase transitions. In the ΔS_M (H, T) map [Fig. 2(f)], the green region (near-zero entropy change) at $T > T_N = 76.5$ K transitioning to blue at higher fields corresponds to the paramagnetic state. The yellow region at $T \approx 76$ K is the phase boundary between the paramagnetic state and the field-induced magnetic state [Fig. 2(f)]. At 74 K $\le T \le$ 76 K and $\mu_0H \ge 0.06$ T, a finite-field positive entropy change (red) of ~0.12 mJ mol^{-1} K^{-1} is ascribed to a metamagnetic phase.

To understand the thermodynamic properties of the ground state of $Fe_2(SeO_3)_3(H_2O)_3$, we performed zero-field specific heat capacity measurements over the range of 2 K $\le T \le$ 300 K [Fig. 3(a)]. The anomalies at $T = 76$ K and $T = 4$ K are consistent with the magnetic transitions in this material. The transition temperature slightly changes under the applied magnetic field 0 T $< \mu_0H <$ 9 T [Fig. 3(b)]. The zero-field specific heat capacity of $Fe_2(SeO_3)_3(H_2O)_3$ can be decomposed into phononic (lattice vibration) and magnetic contributions. To estimate the mean energy accompanying the phonons, the molar heat capacity over temperature C_p/T vs temperature T plot was best described using two Debye modes and one Einstein mode [Eqs. (5)–(7)],[46,47]

$$C_p(T) = C_{D1}(\theta_{D1}, s_{D1}, T) + C_{D2}(\theta_{D2}, s_{D2}, T) + C_E(\theta_E, s_E, T), \tag{5}$$

$$C_D(\theta_D, T) = 9 s_D R\left(\frac{T}{\theta_D}\right)^3 \int_0^{\theta_D/T} \frac{(\theta_D/T)^4 e^{\theta_D/T}}{\left[e^{(\theta_D/T)} - 1\right]^2} d\frac{\theta_D}{T}, \tag{6}$$

$$C_E(\theta_E, T) = 3 s_E R\left(\frac{\theta_E}{T}\right)^2 \frac{e^{\theta_E/T}}{\left[e^{(\theta_E/T)} - 1\right]^2}. \tag{7}$$

θ_{D1} and θ_{D2} are the Debye temperatures; θ_E is the Einstein temperature; s_{D1}, s_{D2}, and s_E are the oscillator strengths; and R is the molar gas constant. The resulting parameters are $s_{D1} = 12.5 \pm 1.5$, $\theta_{D1} = 776 \pm 100$ K, $s_{D2} = 4.9 \pm 1.5$, $\theta_{D2} = 274 \pm 47$ K, $s_E = 4.36(10)$, and $\theta_{E2} = 72 \pm 2$ K. The sum of the oscillators 19(3) is lower than the expected value of 23. This is likely due to the coupling of the high-frequency optical excitations driven by the strong covalent characters of the $(SeO_3)_2$- and H_2O ligands.[48–50]

The entropy recovered from the magnetic transition ΔS_{mag} was estimated after the phonon subtraction using the following equation:

$$\Delta S = \int_0^T \frac{C_V}{T} dT, \tag{8}$$

where C_v is the heat capacity at constant volume, which is approximated to be C_p (heat capacity at constant pressure) for solids at low temperatures, and T is the temperature.[42,51] ΔS_{mag} was estimated to be 21.8(1) J mol^{-1} K^{-1}, which is ~73% of 2 × $[Rln(2S+1)]$ for two Fe^{3+} cations ($S = 5/2$) per formula unit (Fig. S8). The fractional entropy recovery can be attributed to several reasons: (i) the existence of residual fluctuations in the ordered state, (ii) an entropy loss is part of a broad continuum, and (iii) the incomplete phase transition down to $T = 2$ K. We acknowledge, however, that incomplete magnetic transition at $T = 2$ K and lack of appropriate nonmagnetic isostructural material for phonon subtraction may hinder an accurate estimation of magnetic specific heat and entropy change ΔS_{mag} of $Fe_2(SeO_3)_3(H_2O)_3$. The magnetic phase diagram of $Fe_2(SeO_3)_3(H_2O)_3$ is proposed by combining results from magnetic susceptibility, dM/dT, and specific heat capacity as shown in Fig. 4.

To gain insight into the nature of the Fe^{3+} cations, we performed ^{57}Fe Mössbauer spectroscopic studies. ^{57}Fe Mössbauer spectra of $Fe_2(SeO_3)_3(H_2O)_3$ were collected as a function of temperature from $T = 300$ K to $T = 4.2$ K.

16 December 2024 14:27:01

© Author(s) 2024

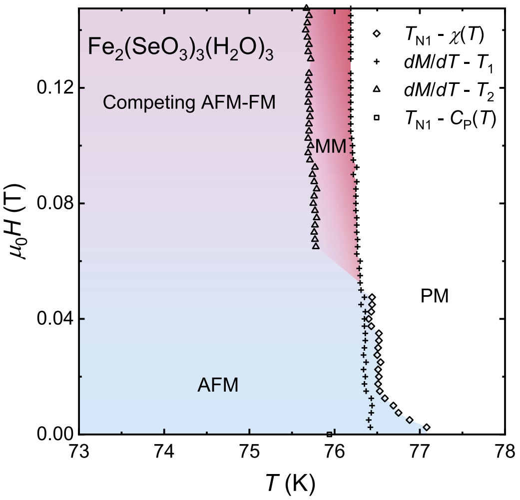

FIG. 4. Proposed magnetic phase diagram of $Fe_2(SeO_3)_3(H_2O)_3$ estimated by combining results from magnetic susceptibility, *dM*/*dT*, and specific heat capacity. AFM: antiferromagnetic, FM: ferromagnetic, PM: paramagnetic, and MM: metamagnetic phase.

As shown in Fig. 5 and Table S5, ^{57}Fe Mössbauer spectra contain two components with almost the same contributions, which correspond to the two Fe sites in the crystal structure, Fe(1) and Fe(2). In the range from $T = 300$ K to $T = 80$ K, the spectral components have the shape of a paramagnetic pseudo-single line with small quadrupole splitting ($\Delta = 0.11$ and 0.05 mm/s at $T = 300$ K) and similar center shifts ($\delta = 0.40$ and 0.44 mm/s at $T = 300$ K). These δ values indicate that the Fe^{3+} cations are high-spin and located in octahedral coordination symmetry. Relatively low values of the quadrupole splitting Δ indicate a fairly regular and symmetrical surrounding of the Fe(1) and Fe(2) sites. The spectral component with a smaller Δ can be assigned to Fe(2). It is owing to a smaller distortion of Fe(2) in the structure [six O atoms of $(SeO_3)^{2-}$ groups] in comparison to Fe(1) linked to three $(SeO_3)^{2-}$ groups and three H_2O molecules [Fig. 1(a)].

^{57}Fe Mössbauer spectra at $T \leq 75$ K show magnetic splitting of distinctly different natures for both components (Fig. 5). The quadrupole couplings have positive signs, and the Δ values in the magnetic state [$\Delta = +0.10$ and +0.07 mm/s at $T = 4.2$ K for Fe(1) and Fe(2), respectively] are close to the values in the paramagnetic state. This indicates that the octahedral coordination environments of Fe(1) and Fe(2) remain unchanged from room temperature to the lowest temperatures.

The spectral component with higher Δ corresponding to Fe(1) indicates a well-defined magnetic structure at $T = 78$ K, as a result of extrapolation shown in Fig. 6(a). A large value of hyperfine magnetic field corresponds to a significant amount of ordered localized magnetic moments for Fe(1) spins. On the other hand, the spectral component with smaller Δ associated with Fe(2) shows the distribution of a hyperfine magnetic field with a relatively small average value down to $T = 30$ K and some kind of magnetic transition at lower temperatures. Close to the ground state (at $T = 4.2$ K), the magnetism of Fe(2) is still distributed, and it can be interpreted as some modulated magnetic structure [Fig. 6(b)]. Temperature evolution of the center shift δ represents a typical second-order Doppler shift dependence on temperature with $\delta = 0.51$ and 0.53 mm/s at $T = 4.2$ K for Fe(1) and Fe(2), respectively. Hence, a suggestion in Ref. 41 about a spin change from Fe^{3+} ($S = 5/2$) to Fe^{2+} ($S = 2$) at low temperatures is not confirmed.

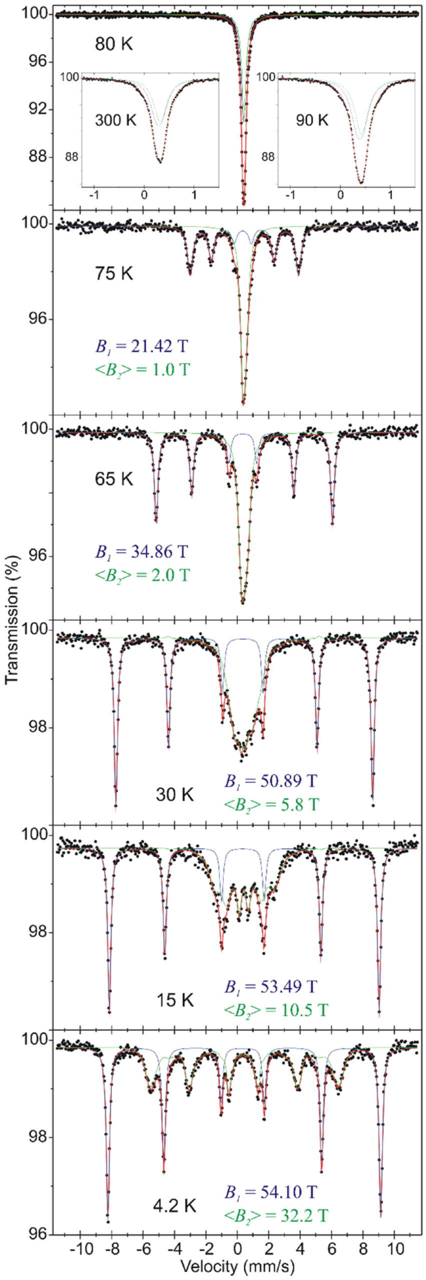

FIG. 5. ^{57}Fe Mössbauer spectra of $Fe_2(SeO_3)_3(H_2O)_3$ vs temperature. The hyperfine magnetic fields for both spectral components are shown.

16 December 2024 14:27:01

© Author(s) 2024

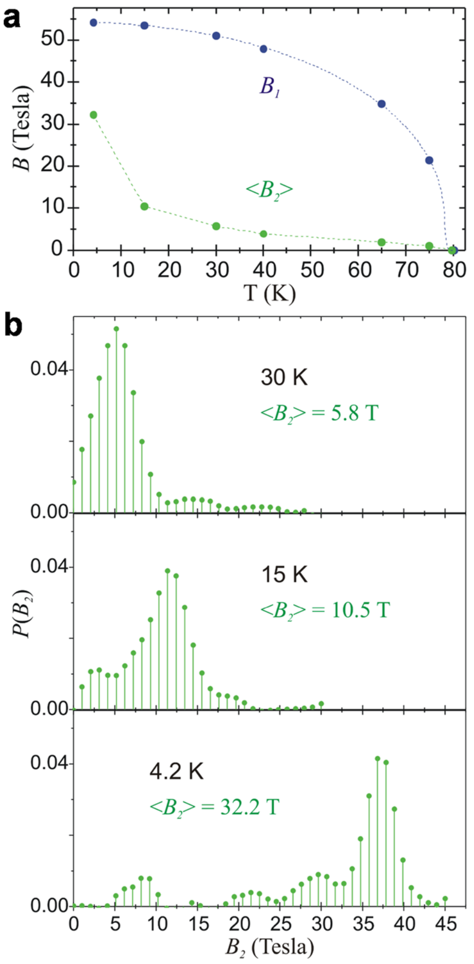

FIG. 6. (a) The hyperfine magnetic field of the magnetically well-defined spectral component, B_1, and the average hyperfine magnetic field of the magnetically distributed spectral component, $<B_2>$, vs temperature. (b) The distribution of magnetic fields $P(B_2)$ (relative probability) as a function of B_2.

To determine the magnetic structure of $Fe_2(SeO_3)_3(H_2O)_3$, we performed single-crystal neutron diffraction on the HB-3A DEMAND at the High Flux Isotope Reactor at Oak Ridge National Laboratory.[54,55] Figures 7(a)–7(c) show the magnetic Bragg peaks of (-1-1-3), (00-3), and (101). Two magnetic transitions were observed in the temperature dependence of (-1-1-3) diffraction intensity at $T \approx 77$ K and $T \approx 10$ K [Fig. 7(d)]. Diffraction data were then collected at $T = 25$ and 5 K to study the magnetic behavior below the phase transitions. In addition to the magnetic peaks with the propagation vector of $k = 0$, indicated by the ordering parameter measurement [Figs. 7(a)–7(c)], no additional magnetic Bragg peaks were observed. So, both transitions result in $k = 0$ magnetic orders, i.e., the ordered magnetic structures have the same unit cell as the crystal structure. From the magnetic symmetry analysis with $k = 0$ and the crystal structure space ($R3c$) utilizing the Bilbao Crystallography Server,[56] multiple magnetic subgroups are possible. The magnetic space groups, including trigonal symmetry, only allow for magnetic moments along the *c*-axis. This symmetry was realized to be inconsistent considering the experimentally observed magnetic reflections such as (00-3) [Fig. 7(b)]. Upon lowering the symmetry, the monoclinic magnetic subgroups Cc' and Cc, which allow in-plane magnetic moment components, were considered for the data refinement.

At $T = 25$ K, the magnetic subgroup Cc yielded the best fitting. There is some correlation between the Fe(1) and Fe(2) sites during magnetic structure refinement. The results from the Mössbauer spectroscopy offered insightful clues to understanding the magnetic behaviors of the Fe(1) and Fe(2) sites. The Fe atoms occupying inequivalent crystallographic sites magnetically order at different temperatures. One Fe site orders at temperature $T \approx 76$ K while the other shows a more distributed magnetic moment. Combining the results from neutron diffraction and Mössbauer spectroscopy experiments, we chose a plausible model for the magnetic structure of $Fe_2(SeO_3)_3(H_2O)_3$. The magnetic moment at the Fe(1) site dominates the magnetic order at $T = 76$ K. A refinement model 1 is constructed with antiparallel Fe^{3+} moments where the magnetic moment of Fe(1) was first refined while constraining the Fe(2) moment to zero. Subsequently, the Fe(2) moment was refined with the Fe(1) moment fixed, resulting in the refined magnetic moment of 4.86(6) μ_B for Fe(1) and 0.9(3) μ_B for Fe(2) at $T = 25$ K [Fig. 7(g)]. The resulting magnetic structure exhibits an antiferromagnetic arrangement of ferrimagnetic Fe(1)–Fe(2) dimers along the *c*-axis, where the orientation of the magnetic moments within each dimer alternates either away or toward the central axis of the dimer. A similar model is used to refine the magnetic structure at $T = 5$ K with magnetic space group Cc.

According to the Mössbauer data, the Fe(1) site is nearly fully ordered at $T = 25$ K; it is reasonable to fix the ordered moment at the Fe(1) site to the high-temperature refined moment of 4.86(6) μ_B when refining the magnetic structure at $T = 5$ K. The refined magnetic moment at the Fe(2) site at $T = 5$ K reaches 2.4(1) μ_B [Fig. 7(h)]. An additional model 2 was also tested, where the Fe(1) moment was constrained to zero at $T = 25$ K to refine the Fe(2) moment, resulting in an ordered moment of 4.84(6) μ_B for Fe(2). The refined parameters from both models are listed in the supplementary material (Table S6). While both models have good refinement, model 1 is chosen to be the magnetic structure of $Fe_2(SeO_3)_3(H_2O)_3$. This can be justified by the combination of both the neutron diffraction and Mössbauer spectroscopy analysis. The local environments of Fe(1) and Fe(2) are chemically different, as proven by the Mössbauer spectroscopy. The neutron data yield the noncollinear magnetic structures of the material at $T = 25$ and 5 K. Thus, connecting the results of the Mössbauer and neutron spectroscopy techniques is vital to arrive at the correct magnetic ordering.

To gain insight into the chemical bonding and orbital overlap in $Fe_2(SeO_3)_3(H_2O)_3$, we performed a spin-polarized density functional theory calculation using the $R3c$ crystal structure (6 formula units) as shown in Fig. 8. The density of state (DOS) plot shows that Fe(1)-*d* and Fe(2)-*d* are polarized, indicating that both Fe sites contribute to magnetism. The Fe^{3+} spins polarize the O-*p*, Se-*s*, Se-*p*, and H-*s* states, giving rise to magnetic exchange interactions. The density of states of Fe(1) and Fe(2) is distinctive, consistent with their behaviors observed in the physical properties, ^{57}Fe Mössbauer spectroscopy, and neutron diffraction. The Fe(1)-*d* states overlap

16 December 2024 14:27:01

© Author(s) 2024

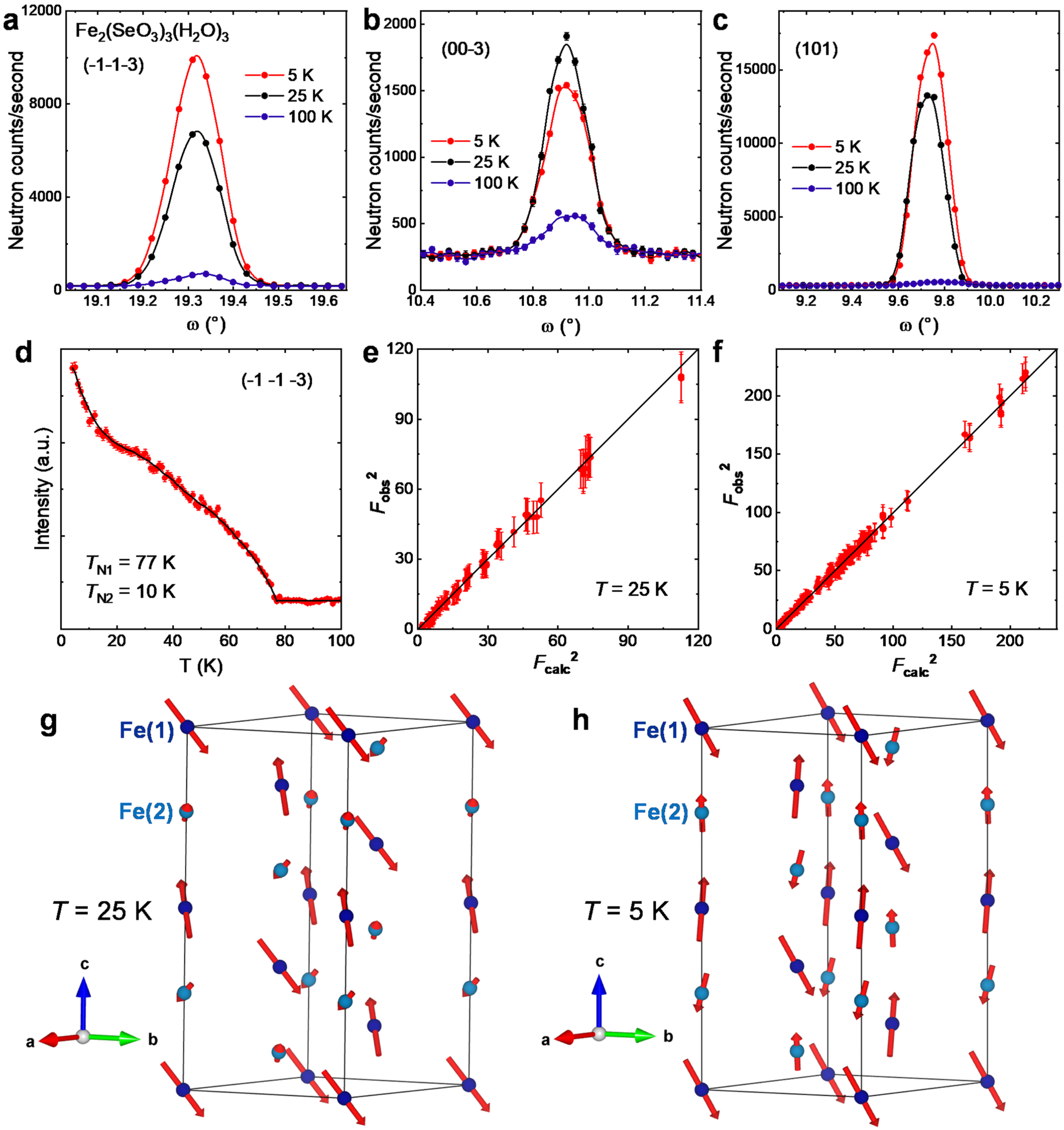

FIG. 7. (a)–(c) Magnetic diffraction of the (-1-1-3), (00-3), and (101) Bragg peaks, respectively. (d) Magnetic diffraction of the (-1-1-3) Bragg peak as a function of temperature showing the antiferromagnetic ordering at T_{N1} = 77 K and T_{N2} ≈ 10 K. (e) and (f) F_{obs} vs F_{calc} plots for the refinement at T = 25 K and T = 5 K, respectively. (g) and (h) The magnetic structure of $Fe_2(SeO_3)_3(H_2O)_3$ at 25 and 5 K, respectively. The fitted spin structure shows ferrimagnetic Fe(1)–Fe(2) dimers along the *c*-axis. The spin moment of Fe(1) is nearly fully ordered at 25 K, while that of Fe(2) is ∼18% ordered. At T = 5 K, the ordered spin moments of Fe(2) approached 50%.

16 December 2024 14:27:01

© Author(s) 2024

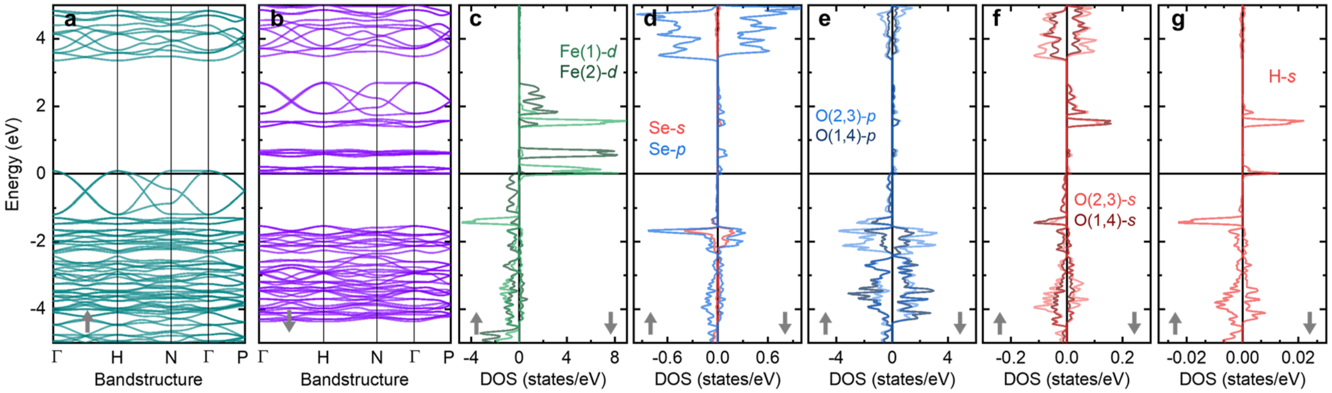

FIG. 8. Spin-polarized band structure and density of states (DOS) of $Fe_2(SeO_3)_3(H_2O)_3$ showing the overlap between Fe-*d*, Se-*s*, Se-*p*, O-*p*, and H-*s* states.

considerably with O(1)-s/*p*, O(4)-s/*p*, and H-*s*, while the Fe(2)-*d* states overlap with O(2)-s/*p* and O(3)-s/*p*. This is consistent with the crystal structure of the compound. The conduction band minimum is mostly composed of Fe(1)-*d*, Se-*p*, O-*p*, and H-*s*, and the valence band maximum is mainly derived from Fe(2)-*d* and O-*p*. In addition to the overlap between the Fe atoms and the ligands, the Fe(1)-*d* and Fe(2)-*d* states also overlap, forming Fe(1)–Fe(2) ferrimagnetic dimers. The DFT computation supports the nontrivial magnetic properties of the material and the contribution of the Fe(1) and Fe(2) spins.

CONCLUSION

Polar magnets with inequivalent magnetic sites offer an exciting avenue for realizing and understanding novel states of matter. In this work, we investigate the complex magnetic behavior of $Fe_2(SeO_3)_3(H_2O)_3$ with two distinct Fe(1) and Fe(2) magnetic sites. At low magnetic fields $\mu_0 H \leq 0.06$ T, this material undergoes antiferromagnetic ordering at $T_{N1} = 77$ K and a second transition at $T_{N2} \approx 4$ K. $Fe_2(SeO_3)_3(H_2O)_3$ displays a metamagnetic transition to spin-polarized states at higher fields. ^{57}Fe Mössbauer spectroscopy and neutron diffraction studies show that the Fe sites behave differently. The spin moment of Fe(1) is nearly fully ordered at $T \approx 25$ K, whereas Fe(2) retains some magnetic frustration down to $T = 4$ K. This results in ferrimagnetic Fe(1)–Fe(2) dimers with an AFM order. DFT computation shows a sufficient overlap between the Fe-*d* and ligand states, supporting the intricate magnetic properties of the system. Further studies, such as field-dependent single-crystal neutron scattering and low-temperature ($T < 2$ K) magnetization and heat capacity measurements, are needed to gain additional insight into the nature of field-induced phase transition and the ground state. The results improve our understanding of the role inequivalent magnetic sites play while enabling more tunable parameters for controlling collective behaviors in polar magnets and altermagnets.

METHODS

Single crystals of $Fe_2(SeO_3)_3(H_2O)_3$ were synthesized by hydrothermal reaction of $FeCl_3 \cdot 6H_2O$ and 2-thenoyl phenyl selenourea (TAS) as described in the supplementary material. Synthesis and characterization of TAS were previously reported.[52,53]

Single crystal crystallographic data of $Fe_2(SeO_3)_3(H_2O)_3$ at $T = 299(2)$ K were collected on a Bruker D8 Venture diffractometer. The structure was solved by intrinsic phasing (SHELXT) and refined by full-matrix least-squares techniques on F^2 (SHELXL) using the SHELXTL software suite.[54] Powder XRD measurements were performed using a Bruker D2 phaser diffractometer with a LynxEye-XE-T detector. Rietveld refinement of the XRD pattern was performed using TOPAS Academic V6. Optical reflectance was measured on $Fe_2(SeO_3)_3(H_2O)_3$ using the Universal Measurement Accessory (UMA) option of the Agilent Cary UV-Vis (NIR) 7000 Spectrophotometer.

DC magnetization measurements on $Fe_2(SeO_3)_3(H_2O)_3$ powder were performed with the vibrating sample magnetometer (VSM) option of the quantum design Physical Properties Measurement System (PPMS). Magnetic susceptibility was approximated as magnetization divided by the applied magnetic field: $\chi \approx M/H$. Heat capacity was measured using the PPMS, employing the semiadiabatic pulse technique from $T = 2$ to 300 K.

^{57}Fe Mössbauer spectroscopy measurements were performed in transmission geometry applying the RENON MsAa-4 spectrometer[55] equipped with the LND Kr-filled proportional detector. The He–Ne laser-based interferometer was used to calibrate a velocity scale. A single-line commercial ^{57}Co(Rh) source was used. A transmission integral approximation has been applied to fit Mössbauer spectra using the MOSGRAF data processing software suite. The spectral isomer (center) shifts δ are reported with respect to the isomer (center) shift of room temperature α-Fe.

Single crystal neutron diffraction on the HB-3A DEMAND[56] at the High Flux Isotope Reactor at Oak Ridge National Laboratory was used to determine the magnetic structure of $Fe_2(SeO_3)_3(H_2O)_3$. The sample was measured at 5 and 25 K with a wavelength of 1.542 Å from a bent Si-220 monochromator.[57] Magnetic symmetry analysis was accomplished using the Bilbao Crystallography Server,[58] considering the propagation *k*-vector and parent space group ($R3c$), while the refinement was performed using the Fullprof software.[59]

16 December 2024 14:27:01

© Author(s) 2024

The spin-polarized density of states and band structure calculations were performed using a full-potential linearized augmented plane wave method as implemented in the WIEN2k code.[60] The exchange and correlation energies were treated within the density functional theory supplemented with Columbic interaction (DFT + U) using the Perdew–Burke–Ernzerhof (PBE) generalized gradient approximation.[61] The muffin-tin radius values of 0.99, 0.83, 0.52, and 0.25 Å were used for Fe, Se, O, and H, respectively. The U for Fe was approximated to be 4.6 eV. The self-consistencies were carried out using a $6 \times 6 \times 6$ k mesh in the irreducible Brillouin zone.

SUPPLEMENTARY MATERIAL

The supplementary material encompasses experimental section, X-ray diffraction data, thermal analysis, FTIR and UV-Vis spectra, additional magnetization and magnetic entropy change, nuclear diffraction Bragg peaks, and ^{57}Fe Mossbauer spectroscopy parameters.

ACKNOWLEDGMENTS

This work was supported by the NSF (Award Nos. NSF-DMR-2338014 and NSF-OIA-2227933). X.H. and T.T.T. thank the Arnold and Mabel Beckman Foundation (2023 BYI grant to T.T.T.) for the support. M.M. and H.C. thank the U.S. DOE Office of Science, Office of Basic Energy Sciences, Early Career Research Program Award No. KC0402020, under Contract No. DE-AC05-00OR22725. Research at Gdansk University of Technology was supported by the National Science Center (Poland) under SONATA-15 (Grant No. 2019/35/D/ST5/03769). A portion of this research used resources at the High Flux Isotope Reactor, a DOE Office of Science User Facility operated by the Oak Ridge National Laboratory. The use of the Advanced Photon Source at Argonne National Laboratory was supported by the US Department of Energy, Office of Science, Office of Basic Energy Sciences, under Contract No. DE-AC02-06CH11357. This manuscript has been authored by UT-Batelle, LLC, under Contract No. DE-AC05-00OR22725 with the US Department of Energy (DOE). The US government retains, and the publisher, by accepting the article for publication, acknowledges that the US government retains a nonexclusive, paid-up, irrevocable, world-wide license to publish or reproduce the published form of this manuscript or allow others to do so, for US government purposes. DOE will provide public access to these results of federally sponsored research in accordance with the DOE Public Access Plan (http://energy.gov/downloads/doe-public-access-plan). Mössbauer measurements were performed by AB using equipment of the Mössbauer Spectroscopy Laboratory, Pedagogical University, Kraków, Poland.

AUTHOR DECLARATIONS

Conflict of Interest

The authors have no conflicts to disclose.

Author Contributions

Ebube E. Oyeka: Data curation (equal); Formal analysis (equal); Investigation (equal); Methodology (equal); Software (equal); Validation (equal); Visualization (lead); Writing – original draft (lead). **Xudong Huai**: Formal analysis (supporting); Software (supporting); Validation (equal); Visualization (supporting). **Madalynn Marshall**: Data curation (equal); Formal analysis (equal); Methodology (equal); Validation (equal); Visualization (equal); Writing – original draft (equal). **Michał J. Winiarski**: Methodology (equal); Resources (equal); Validation (equal); Writing – review & editing (equal). **Artur Błachowski**: Data curation (equal); Formal analysis (equal); Investigation (equal); Methodology (equal); Resources (equal); Validation (equal); Visualization (equal); Writing – review & editing (equal). **Huibo Cao**: Data curation (equal); Formal analysis (equal); Investigation (equal); Methodology (equal); Resources (equal); Validation (equal); Writing – original draft (equal); Writing – review & editing (equal). **Thao T. Tran**: Conceptualization (lead); Funding acquisition (lead); Project administration (lead); Resources (lead); Validation (lead); Writing – review & editing (lead).

DATA AVAILABILITY

The data that support the findings of this study are available within the article and its supplementary material.

REFERENCES

[1] J. Junquera, Nat. Mater. **20**, 291 (2021).

[2] X. Zhang *et al.*, J. Phys. Condens. Matter **32**, 143001 (2020).

[3] Q. L. He, T. L. Hughes, N. P. Armitage, Y. Tokura, and K. L. Wang, Nat. Mater. **21**, 15 (2022).

[4] S.-H. Yang, R. Naaman, Y. Paltiel, and S. S. P. Parkin, Nat. Rev. Phys. **3**, 328 (2021).

[5] C.-H. Hsu, P. C. Sreeparvathy, C. K. Barman, F.-C. Chuang, and A. Alam, Phys. Rev. B **103**, 195143 (2021).

[6] S. Roychowdhury, S. Singh, S. N. Guin, N. Kumar, T. Chakraborty, W. Schnelle, H. Borrmann, C. Shekhar, and C. Felser, Chem. Mater. **33**, 8343 (2021).

[7] N. Kanazawa, S. Seki, and Y. Tokura, Adv. Mater. **29**, 1603227 (2017).

[8] Y. Tokura and N. Kanazawa, Chem. Rev. **121**, 2857 (2021).

[9] S. Mühlbauer, B. Binz, F. Jonietz, C. Pfleiderer, A. Rosch, A. Neubauer, R. Georgii, and P. Böni, Science **323**, 915 (2009).

[10] K. Lu, D. Sapkota, L. DeBeer-Schmitt, Y. Wu, H. B. Cao, N. Mannella, D. Mandrus, A. A. Aczel, and G. J. MacDougall, Phys. Rev. Mater. **4**, 054416 (2020).

[11] Y. Araki *et al.*, Phys. Rev. B **102**, 054409 (2020).

[12] J. W. Kim *et al.*, Phys. Rev. Lett. **115**, 137201 (2015).

[13] Y. S. Tang *et al.*, Phys. Rev. B **103**, 014112 (2021).

[14] F. J. dos Santos, M. dos Santos Dias, and S. Lounis, Phys. Rev. B **102**, 104401 (2020).

[15] S.-W. Cheong and M. Mostovoy, Nat. Mater. **6**, 13 (2007).

[16] D. A. Sokolov *et al.*, Nat. Phys. **15**, 671 (2019).

[17] J. H. Lee and R. S. Fishman, Phys. Rev. Lett. **115**, 207203 (2015).

[18] H. Murakawa, Y. Onose, and Y. Tokura, Phys. Rev. Lett. **103**, 147201 (2009).

[19] T. T. Ly *et al.*, Adv. Funct. Mater. **31**, 2009758 (2021).

[20] M. Marshall, B. R. Billingsley, X. Bai, Q. Ma, T. Kong, and H. Cao, Nat. Commun. **14**, 3641 (2023).

[21] L. Ding *et al.*, Nat. Commun. **12**, 5339 (2021).

[22] E. Stryjewski and N. Giordano, Adv. Phys. **26**, 487 (1977).

[23] N. Kikugawa, D. A. Sokolov, C. Sow, Y. Maeno, and A. P. Mackenzie, J. Phys. Soc. Jpn. **90**, 103704 (2021).

[24] A. W. Rost, R. S. Perry, J. F. Mercure, A. P. Mackenzie, and S. A. Grigera, Science **325**, 1360 (2009).

[25] W. Bao, Z. Q. Mao, Z. Qu, and J. W. Lynn, Phys. Rev. Lett. **100**, 247203 (2008).

[26] E. E. Oyeka, M. J. Winiarski, A. Błachowski, K. M. Taddei, A. Scheie, and T. T. Tran, Chem. Mater. **33**, 4661 (2021).

16 December 2024 14:27:01

© Author(s) 2024

[27] T. Kurumaji, S. Ishiwata, and Y. Tokura, Phys. Rev. X **5**, 031034 (2015).

[28] Y. Wang, G. L. Pascut, B. Gao, T. A. Tyson, K. Haule, V. Kiryukhin, and S.-W. Cheong, Sci. Rep. **5**, 12268 (2015).

[29] S. Seki, X. Z. Yu, S. Ishiwata, and Y. Tokura, Science **336**, 198 (2012).

[30] J.-W. G. Bos, C. V. Colin, and T. T. M. Palstra, Phys. Rev. B **78**, 094416 (2008).

[31] S.-H. Kim, P. S. Halasyamani, B. C. Melot, R. Seshadri, M. A. Green, A. S. Sefat, and D. Mandrus, Chem. Mater. **22**, 5074 (2010).

[32] T. Kurumaji, T. Nakajima, V. Ukleev, A. Feoktystov, T.-h. Arima, K. Kakurai, and Y. Tokura, Phys. Rev. Lett. **119**, 237201 (2017).

[33] S. J. R. Holt, C. Ritter, M. R. Lees, and G. Balakrishnan, J. Phys.: Condens. Matter **33**, 255802 (2021).

[34] I. Kézsmárki *et al.*, Nat. Mater. **14**, 1116 (2015).

[35] Y. Yoshida, S.-I. Ikeda, H. Matsuhata, N. Shirakawa, C. H. Lee, and S. Katano, Phys. Rev. B **72**, 054412 (2005).

[36] S. Reschke, A. A. Tsirlin, N. Khan, L. Prodan, V. Tsurkan, I. Kézsmárki, and J. Deisenhofer, Phys. Rev. B **102**, 094307 (2020).

[37] T. Kurumaji, Y. Takahashi, J. Fujioka, R. Masuda, H. Shishikura, S. Ishiwata, and Y. Tokura, Phys. Rev. B **95**, 020405 (2017).

[38] K. J. A. Franke, P. R. Dean, M. C. Hatnean, M. T. Birch, D. D. Khalyavin, P. Manuel, T. Lancaster, G. Balakrishnan, and P. D. Hatton, AIP Adv. **9**, 125228 (2019).

[39] A. Štefančič, S. J. R. Holt, M. R. Lees, C. Ritter, M. J. Gutmann, T. Lancaster, and G. Balakrishnan, Sci. Rep. **10**, 9813 (2020).

[40] R. L. Dally *et al.*, Phys. Rev. B **102**, 014410 (2020).

[41] A. Larrañaga, J. L. Mesa, J. L. Pizarro, L. Lezama, M. I. Arriortua, and T. Rojo, Spectrochim. Acta, Part A **69**, 1020 (2008).

[42] M. J. Winiarski, T. T. Tran, J. R. Chamorro, and T. M. McQueen, Inorg. Chem. **58**, 4328 (2019).

[43] M.-H. Yu, L. H. Lewis, and A. R. Moodenbaugh, J. Appl. Phys. **93**, 10128 (2003).

[44] P. Lampen, N. S. Bingham, M. H. Phan, H. Srikanth, H. T. Yi, and S. W. Cheong, Phys. Rev. B **89**, 144414 (2014).

[45] C. Triguero, M. Porta, and A. Planes, Phys. Rev. B **76**, 094415 (2007).

[46] A. Tari, *The Specific Heat of Matter at Low Temperatures* (Published by Imperial College Press and distributed by World Scientific Publishing Co., 2003).

[47] T. Berry, L. A. Pressley, W. A. Phelan, T. T. Tran, and T. M. McQueen, Chem. Mater. **32**, 5827 (2020).

[48] E. E. Oyeka, M. J. Winiarski, H. Świątek, W. Balliew, C. D. McMillen, M. Liang, M. Sorolla II, and T. T. Tran, Angew. Chem., Int. Ed. **61**, e202213499 (2022).

[49] J. Kondek, S. Szczupaczyńska-Zalewska, and M. J. Winiarski, J. Magn. Magn. Mater. **562**, 169794 (2022).

[50] T. Jia, J. Carrete, Z. Feng, S. Guo, Y. Zhang, and G. K. Madsen, Phys. Rev. B **102**, 125204 (2020).

[51] V. Fritsch, N. O. Moreno, J. D. Thompson, J. L. Sarrao, and S. Bobev, J. Magn. Magn. Mater. **299**, 87 (2006).

[52] E. E. Oyeka and T. T. Tran, ACS Org. Inorg. Au **2**, 502 (2022).

[53] M. Musthafa, R. Konakanchi, R. Ganguly, C. Balachandran, S. Aoki, and A. Sreekanth, J. Biomol. Struct. Dyn. **39**, 4346 (2021).

[54] G. M. Sheldrick, Acta Crystallogr., Sect. C:Struct. Chem. **71**, 3 (2015).

[55] A. Błachowski, K. Ruebenbauer, J. Żukrowski, and R. Górnicki, Acta Phys. Pol. A **114**, 1707 (2008).

[56] H. Cao *et al.*, Crystals **9**(5), 256 (2019).

[57] B. C. Chakoumakos *et al.*, J. Appl. Crystallogr. **44**, 655 (2011).

[58] J. M. Perez-Mato, S. V. Gallego, E. S. Tasci, L. Elcoro, G. de la Flor, and M. I. Aroyo, Annu. Rev. Mater. Res. **45**, 217 (2015).

[59] J. Rodríguez-Carvajal, Physica B **192**, 55 (1993).

[60] P. Blaha, K. Schwarz, F. Tran, R. Laskowski, G. K. H. Madsen, and L. D. Marks, J. Chem. Phys. **152**, 074101 (2020).

[61] J. P. Perdew, K. Burke, and M. Ernzerhof, Phys. Rev. Lett. **77**, 3865 (1996).

16 December 2024 14:27:01

© Author(s) 2024